Front. Mech. Eng. 2017, 12(1): 110–115
DOI 10.1007/s11465-017-0430-5

RESEARCH ARTICLE

Mingjin XU, Yifan DAI, Xuhui XIE, Lin ZHOU, Shengyi LI, Wenqiang PENG

Ion beam figuring of continuous phase plates based on the frequency filtering process

Abstract Ion beam figuring (IBF) technology is an effective technique for fabricating continuous phase plates (CPPs) with small feature structures. This study proposes a multi-pass IBF approach with different beam diameters based on the frequency filtering method to improve the machining accuracy and efficiency of CPPs during IBF. We present the selection principle of the frequency filtering method, which incorporates different removal functions that maximize material removal over the topographical frequencies being imprinted. Large removal functions are used early in the fabrication to figure the surface profile with low frequency. Small removal functions are used to perform final topographical correction with higher frequency and larger surface gradient. A high-precision surface can be obtained as long as the filtering frequency is suitably selected. This method maximizes the high removal efficiency of the large removal function and the high corrective capability of the small removal function. Consequently, the fast convergence of the machining accuracy and efficiency can be achieved.

Keywords ion beam figuring (IBF), continuous phase plates (CPPs), machining accuracy, machining efficiency, frequency filtering process

1 Introduction

Continuous phase plate (CPP) with continuously varying topographical features is a typical diffractive optical element that has been extensively applied in high-power laser systems [1,2]. In recent years, high-precision fabrication of CPPs with complex and irregular 3D microstructures has been required. The Lawrence Livermore National Laboratory developed a magnetorheological finishing (MRF) to process a large-aperture CPP (430 mm×430 mm), and the machining precision reached 30 nm root-mean-square (RMS) [3,4]. Chemical etching was adopted to fabricate a CPP (383 mm×398 mm) in the French Laser Integration Line [5]. The advantage of MRF and chemical etching methods lies in their high efficiency in processing large-aperture CPPs. However, due to the size limitation of polishing tools, the high-precision fabrication of CPPs with small feature structures (smaller than 4 mm) and large surface gradient (approximately larger than 1 μm/cm) remains difficult to achieve. Xu et al. [6] developed the ion beam moving etching technology for the fabrication of diffractive optical elements; however, masks in the *x*- and *y*-direction are both needed, which is not suitable for complex phase structures. The high-precision fabrication of CPPs with small feature structures and large surface gradient has become a critical problem. Ion beam figuring (IBF) based on the physical sputtering effect is used for the machining of nano- or sub-nanometer precision surface accuracy and super-smooth surface quality [7,8]. Moreover, the polishing tool cannot adapt to arbitrary surface changes during traditional polishing process; this problem can be solved by using different sizes of ion beam removal function, whose beam diameter can be easily reduced to 1 mm or smaller [9]. Consequently, IBF technology provides a new possible solution for the high-precision fabrication of CPPs with small characteristic dimensions.

We have fabricated CPPs with characteristic dimensions as small as 1.5 mm and surface peak-to-valleys (PV) as small as 166 nm to within 10 nm RMS of design specifications. However, previous figuring experiments show that certain limitations exist in the adoption of the traditional IBF process directly used for plane or curved surface to machine CPPs. Large errors between the figured

Received July 29, 2016; accepted December 26, 2016

Mingjin XU, Yifan DAI, Xuhui XIE (✉), Lin ZHOU, Shengyi LI
College of Mechatronics Engineering and Automation, National University of Defense Technology, Changsha 410073, China
E-mail: xuhuixie67@sina.com

Wenqiang PENG
College of Basic Education for Command Officer, National University of Defense Technology, Changsha 410073, China

surface and the desired CPP surface still exist after several figuring iterations. Moreover, the residual surface errors become time-consuming when they gradually tend to be mid-to-high spatial frequencies. Therefore, the figuring process optimization needs to be analyzed to improve machining precision and efficiency. This paper presents a multi-pass IBF approach with different beam diameters based on the frequency filtering method. We describe the advantages of the frequency filtering method over the direct figuring method by comparing the simulated results, which can guide the actual figuring process.

2 Problems during IBF

The figuring principle of CPPs by IBF technology is similar to that of the MRF [3,4]. Previous research and analysis of our exploratory experiments show that the reasons for the low-precision and low-efficiency fabrication of CPPs by IBF are due to the surface topography of feature structures and the adaptability of IBF removal function. The desired CPP surface is different from that of a plane or sphere surface, which appears as a mountainous area with ups and downs. The existence of slopes and pits leads to inadaptability to mid-to-high spatial frequency ranges for the ion beam. Thus, even minor machining errors can be accumulated, amplified, and directly affect the entire figuring process. The machining precision and efficiency is significantly affected by the removal function size. Large errors will be introduced by a large IBF removal function, and more dwell time is needed by a small ion beam. These problems must be solved to balance the precision and efficiency.

Reference [10] presents the cut-off corrective frequency (f_c) to quantitatively evaluate the corrective capability of the IBF removal function.

$$f_c = \frac{3\sqrt{2\ln 10}}{\pi d_{6\sigma}}. \tag{1}$$

Therefore, the required beam diameter ($d_{6\sigma}$) to imprint characteristic dimensions with certain spatial wavelength is

$$d_{6\sigma} \leqslant \frac{3\sqrt{2\ln 10}}{\pi}\frac{1}{f_c} \approx 2\lambda_c, \tag{2}$$

where $\lambda = 1/f$ is the spatial wavelength of feature structures.

Equation (2) indicates that CPPs with smaller characteristic dimensions can be figured by decreasing the ion beam diameter. A small beam diameter implies that small feature structures can be imprinted. However, the volume removal rate of ion beam decreases dramatically with the reduction of beam diameter, thereby sharply increasing the dwell time of a small beam. Figure 1 shows the simulation results of dwell time varying with removal depth under different beam diameters. Results show that the dwell time required by a small beam is significantly greater than that of a big beam with the increase of material removal. Therefore, the removal function should be rationally selected and arranged during different machining stages to balance the machining precision and efficiency and thus achieve high-precision results.

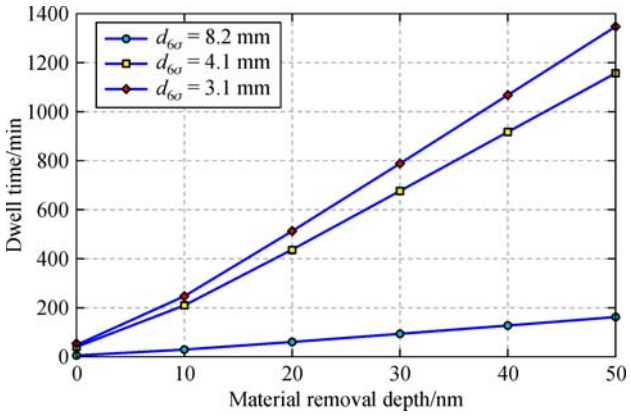

Fig. 1 Relationship between dwell time and material removal depth under different beam diameters

3 Figuring process optimization

3.1 Multi-pass IBF under different beam diameters

The feature structures gradually tend to be mid-to-high spatial frequencies when the figured surface is near the desired CPP surface. However, the removal function sizes essentially limit the sampling bandwidth of the feature structures due to Nyquist critical sampling issues [3]. The attempt to imprint smaller feature structures (higher frequencies) than the smallest practical removal function dimensions (cut-off corrective frequency) results in longer polishing times and greater material removal because less removal function is effectively used for imprinting the topography. Thus, the machining precision and efficiency can be balanced by selecting a reasonable removal function. The figuring process can be planned by combining the corrective capability of the removal function and the spatial frequency analysis of feature structures. The figuring process controls dwell time and adequately exerts the corrective capability of the used removal function.

For a given removal function, the machining efficiency is different for feature structures with different spatial frequencies. The figuring convergence rate is rapid for low frequencies and negligible near the cut-off corrective frequency. Liao et al. [10] presented a selection principle for different removal functions, which can be a good reference in the current study. The surface error ratio for evaluating the degree of figuring difficulty can be expressed as:

$$k = \frac{\mathrm{RMS_e}}{\mathrm{RMS_{he}}}, \quad (3)$$

where $\mathrm{RMS_e}$ is the RMS of the entire spatial frequency error, and $\mathrm{RMS_{he}}$ is the RMS of the spatial errors whose frequency is higher than the cut-off corrective frequency.

A larger k implies a high surface accuracy that is easier to reach. However, it takes more dwell time. The rational value of k is set between 2 and 6 to balance machining efficiency and precision. The selected value should be relatively large in the rough machining stage and small in the finish machining stage, so the total machining convergence ratio can be quickly improved. When k is at 1.5 after several reiterations, the removal function should be changed to a smaller one. The selected removal functions according to the value of k and the arrangements of dwell time and iterative numbers in figuring experiments of CPP are shown in Tables 1 and 2, respectively. Tables 1 and 2 describe the two machining stages in which two beams with diameters of 8.2 and 4.1 mm are used. The first stage is the rough figuring, with a beam of $d_{6\sigma}$= 8.2 mm used to achieve the rapid correction of low-frequency errors. After two iterations, the surface error ratio is k = 1.46, indicating that the removal function has little effective corrective capability. The second stage is finishing machining (Table 2). The matching error between the desired surface and the figured surface is gradually evolved into mid-to-high frequency components, and thus a smaller ion beam is required to improve figuring precision.

3.2 Frequency filtering method

The frequency filtering process, which is an improvement of the multi-pass IBF process under different beam diameters, aims to achieve high machining efficiency and precision. The morphological changes of the microstructure with different spatial frequencies are quite different. Moreover, this difference leads to completely different error patterns when the same removal function is used. Thus, the problems of the machining precision and efficiency cannot be thoroughly solved simply by the multi-pass IBF process.

To solve this problem, we apply the frequency filtering process into the fabrication of CPPs. High surface accuracy can be achieved by iterative machining of the filtered surface, because the actual machining error is small due to the lack of high-frequency components. If the matching error between the filtered surface and the desired surface is E_1, and the machining error of the filtered surface is E_2, then the total error of the frequency filtering process is E_1+ E_2. The machining error from the direct machining of the desired surface is assumed to be E_0. In the CPP process with a sharp morphological change, machining error E_2 will be significantly lesser than E_0, and the matching error E_1 also can be controlled to be small. The effect of E_1+ $E_2 < E_0$ is likely to be achieved in the actual CPP figuring process.

Based on this idea, a Gaussian low-pass filter is selected to filter the mid-to-high spatial frequency during fabrication. The desired CPP surface is shown in Fig. 2(a); and Fig. 2(b) presents the filtered surface by a Gaussian low-pass filter with 4 mm bandwidth. The comparison of Figs. 2(a) and 2(b) shows that the high-frequency components have been filtered out, and a relatively smooth surface with low-frequency is obtained. First, the filtered surface underwent virtual simulation with a large ion beam, and the total machining error is processed with a small ion beam. The matching error is shown in Fig. 2(c), and the error value is 124.9 nm PV, 11.3 nm RMS. The machining error of the filtered surface is 24.9 nm PV, 2.9 nm RMS, when a beam of $d_{6\sigma}$= 8.2 mm is used, as shown in Fig. 2(d). The total error of the frequency filtering process is 143.2 nm PV, 13.8 nm RMS, which is the superposition of the matching error and the machining error, as shown in Fig. 2(e). However, the machining error from the direct machining method by the same removal function is 155.0 nm PV, 16.6 nm RMS, as shown in Fig. 2(f). Simulation results show that the machining error obtained by the frequency filtering process has a small PV and RMS value; therefore, it is essential in achieving a high-precision result.

Table 1 First figuring stage (beam diameter $d_{6\sigma}$= 8.2 mm and f_c= 0.25 $\mathrm{mm^{-1}}$)

Arrangement of dwell time	Surface error, PV/nm	Surface error, RMS/nm	Surface error, $\mathrm{PV_{he}}$/nm	Surface error, $\mathrm{RMS_{he}}$/nm	k
Before IBF	198.7	27.4	122.3	11.3	2.42
After 1st IBF	171.0	16.5	119.3	10.3	1.60
After 2nd IBF	168.5	14.6	120.5	10.0	1.46

Table 2 Second figuring stage (beam diameter $d_{6\sigma}$= 4.1 mm and f_c= 0.5 $\mathrm{mm^{-1}}$)

Arrangement of dwell time	Surface error, PV/nm	Surface error, RMS/nm	Surface error, $\mathrm{PV_{he}}$/nm	Surface error, $\mathrm{RMS_{he}}$/nm	k
Before IBF	168.5	14.6	72.6	5.1	2.86
After 1st IBF	160.7	13.3	72.0	5.0	2.66
After 2nd IBF	153.4	12.7	71.0	4.9	2.59

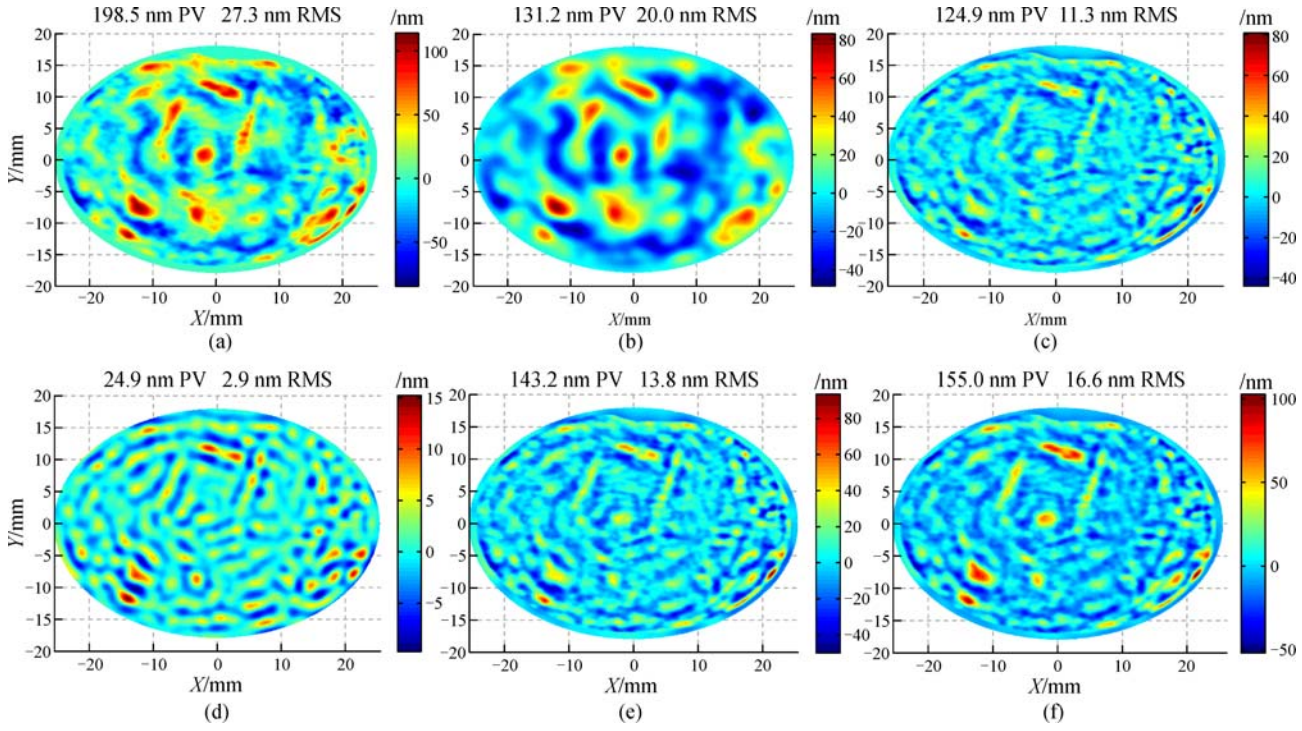

Fig. 2 Comparison of machining errors of the two figuring processes: (a) The desired CPP surface; (b) the filtered surface by a Gaussian low-pass filter with 4 mm bandwidth; (c) the matching error; (d) the machining error of the filtered surface; (e) the total error of the frequency filtering process; (f) the total error of the direct figuring process

In addition, the frequency filtering process can improve the machining efficiency, especially for surface errors rich in mid-to-high frequencies. This reason is that the dwell time algorithm of IBF is based on the principle of obtaining nanometer precision surface, without considering the effect of machining efficiency. Surface errors of all frequency ranges will affect the dwell time calculation results, leading to a significant increase of dwell time. As shown in Fig. 3, taking the matching error between the figured surface and desired surface as an example, the residual machining error of the filtered surface by a Gaussian low-pass filter with 2 mm bandwidth is 100.8 nm PV, 6.5 nm RMS, which is machined by a beam of $d_{6\sigma}$= 4.1 mm and under a total figuring time of T_1= 450 min. The residual machining error of the direct machining process is 105.3 nm PV, 6.3 nm RMS, and the figuring time is T_2= 640 min, as shown in Table 3. Although the residual machining errors of the two process methods are similar, the frequency filtering process can save approximately 30% of the total figuring time.

The multi-pass IBF process based on the frequency filtering incorporates different removal functions that maximize material removal over the topographical frequencies being imprinted. Large removal functions are used to figure the surface profile of low frequency. Small

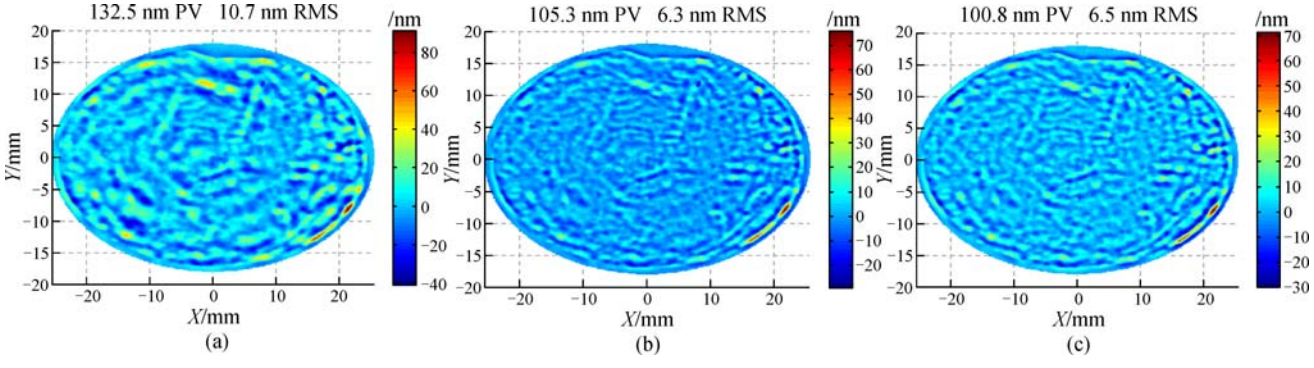

Fig. 3 Comparison of surface errors figured by the two figuring processes: (a) The original surface error; (b) surface error of the direct machining process; (c) surface error of the frequency filtering process

Table 3 Comparison of machining time by the two process methods (beam diameter $d_{6\sigma}$= 4.1 mm)

Process method	Surface error, PV/nm	Surface error, RMS/nm	Figuring time/min	Time reduced
IBF before filter	105.3	6.3	640	
IBF after filter	100.8	6.5	450	30%

removal functions perform final topographical correction on high-frequency and large-surface gradients. A high-precision surface can be obtained as long as a suitable filtering frequency is selected. This method maximizes the high removal efficiency of the large removal function and the high corrective capability of the small removal function. Consequently, this approach improves the machining efficiency and achieves fast convergence of machining precision.

4 Figuring experiments

Figure 4 shows the CPP surface morphology to be processed, whose PV is approximately 200 nm and the maximum surface gradient is 3.1 μm/cm found only on the surface edge. All figuring experiments are performed in our self-developed IBF systems (2.5×10^{-3} Pa pressure) under the bombardment of Ar^{+} ions at normal incidence. Within the experiments, the figuring conditions are fixed at

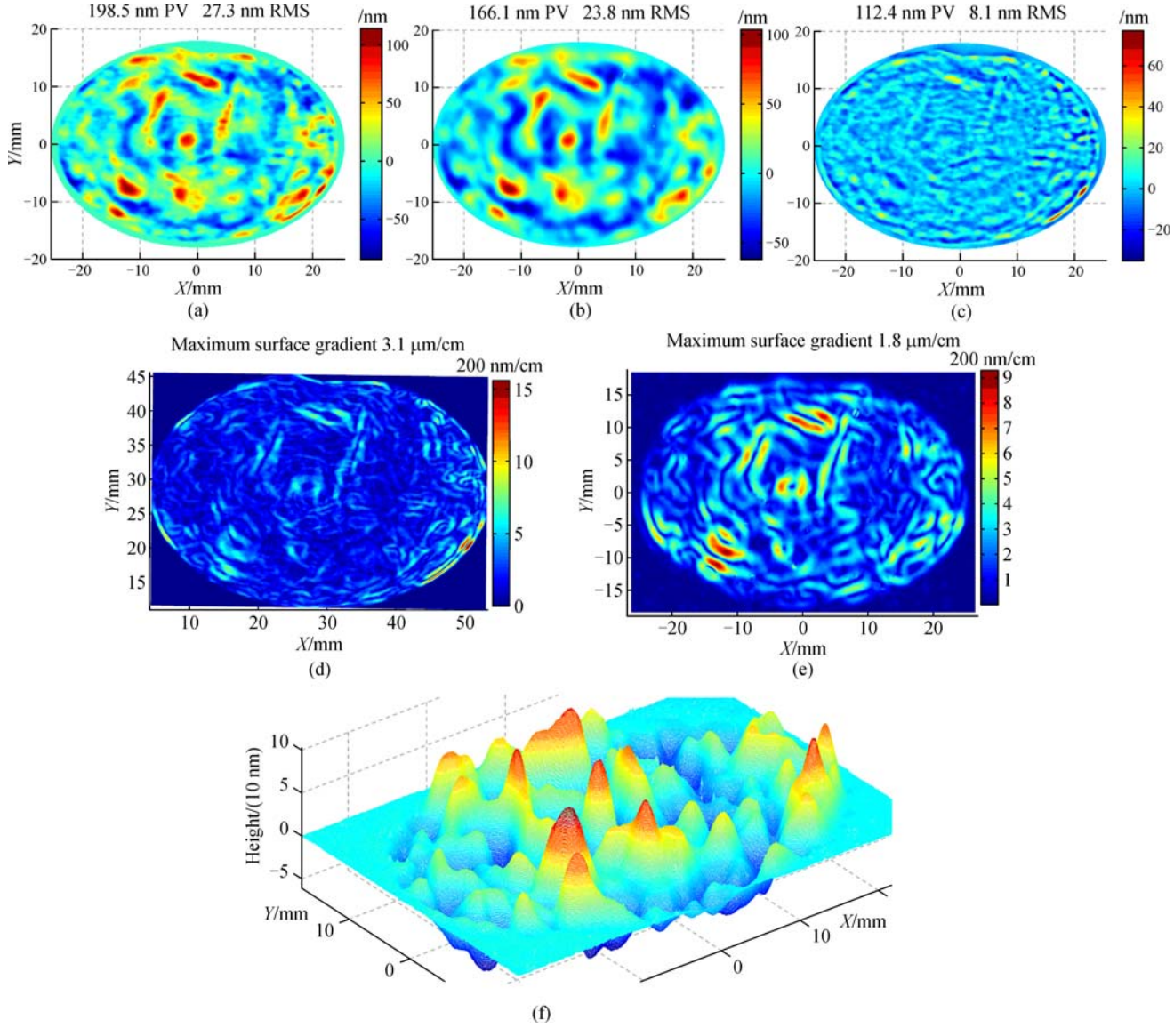

Fig. 4 Surface accuracy of the figured CPP: (a) The desired CPP surface; (b) the figured CPP surface; (c) the final matching error; (d) surface gradient distribution of the desired CPP; (e) surface gradient distribution of the figured CPP; (f) 3D view of the figured CPP

an ion source energy E_{ion}= 800 eV and beam current J_{ion}= 25 mA.

Figure 4 shows that the surface accuracy of the figured CPP is 23.8 nm RMS, 166.1 nm PV, and the final matching error between the actual figured surface and the desired CPP surface is 8.1 nm RMS, 112.4 nm PV. The PV of matching errors is not a good metric for assessing the quality of the imprinting. The optic appears worse than it actually is, because PV is computed from only two data points out of a possible thousand. The RMS calculated from all the data on the optical surface indicates the overall optic performance better. The imprinting error stems from minor mismatches near the peaks and valleys where collateral polishing causes feature washout because of a large slope gradient. The comparison of Figs. 4(d) and 4(e) shows that the surface gradient that can be imprinted reaches approximately 1.8 μm/cm, which has the same distribution with the desired CPP surface apart from the surface edge.

5 Summary

Complex surface topography and rich mid-to-high frequency error components restrict the fast convergence of machining accuracy and efficiency of CPPs during IBF. A multi-pass IBF approach with different beam diameters based on the frequency filtering method is proposed to solve this problem. The principle of the frequency filtering method incorporates different removal functions that maximize material removal and corrective capability over the topographical frequencies being imprinted. Large removal functions are used to achieve the large material removal, and small removal functions are used to improve figuring precision in the fabrication. Simulation results show that a high-precision surface can be obtained and less machining time is needed as long as the suitable filtering frequency is selected. This method maximizes the high removal efficiency of the large removal function and the high corrective capability of the small removal function. The final figuring experiment results of the CPP prove the peculiarity of our strategy.

Acknowledgements We gratefully acknowledge the support of the National Natural Science Foundation of China (Grant Nos. 91323302 and 61505259) and the Program for New Century Excellent Talents in University (NCET-13-0165).

References

1. Menapace J A, Davis P J, Steele W A, et al. MRF applications: On the road to making large-aperture ultraviolet laser resistant continuous phase plate for high-power lasers. Proceedings of the Society for Photo-Instrumentation Engineers, 2006, 6403: 64030N
2. Néauport J, Ribeyre X, Daurios J, et al. Design and optical characterization of a large continuous phase plate for laser integration line and laser megajoule facilities. Applied Optics, 2003, 42(13): 2377–2382
3. Menapace J A, Dixit S N, Genin F Y, et al. Magnetorheological finishing for imprinting continuous phase plate structure onto optical surfaces. Proceedings of the Society for Photo-Instrumentation Engineers, 2004, 5273: 220–230
4. Tricard M, Dumas P, Menapace J. Continuous phase plate polishing using Magnetorheological Finishing. Proceedings of the Society for Photo-Instrumentation Engineers, 2008, 7062: 70620V
5. Beau V, Valla D, Daurios J, et al. Metrology of focusing gratings and continuous phase plates for LIL and LMJ lasers. Proceedings of the Society for Photo-Instrumentation Engineers, 2004, 5252: 148–155
6. Xu J, Zhao Y, Wang W, et al. Design and fabrication of diffractive optical elements for ion beam moving etching technology. Optics Technology, 2002, 28(4): 345–350
7. Xu M, Dai Y, Xie X, et al. Structure optimization and fabricating capability analysis of an ion-beam machine for sub-nanometer optical surface. Applied Optics, 2015, 54(27): 8055–8061
8. Liao W, Dai Y, Xie X, et al. Microscopic morphology evolution during ion beam smoothing of Zerodur® surfaces. Optics Express, 2014, 22(1): 377–386
9. Hansel T, Nickel A, Schindler A. Ion beam figuring of strongly curved surfaces with a (X, Y, Z) linear three-axes system. In: Frontiers in Optics 2008/Laser Science XXIV/Plasmonics and Metamaterials/Optical Fabrication and Testing. 2008, JWD6
10. Liao W, Dai Y, Xie X, et al. Corrective capability analysis and machining error control in ion beam figuring of high-precision optical mirrors. Optical Engineering, 2012, 51(3): 033402